105
123

Longitudinal Misalignment Based Strain Sensor

by

Jeffrey Pratt Andrews

Thesis submitted to the Faculty of the

Virginia Polytechnic Institute and State University

in partial fulfillment of the requirements for the degree of

Masters of Science

in

Electrical Engineering

APPROVED:

Richard O. Claus

Richard O. Claus, Chairman

Gary S. Brown

Ronald J. Pieper

Longitudinal Misalignment Based Strain Sensor

by

Jeffrey Pratt Andrews

Richard O. Claus, Chairman

Electrical Engineering

(ABSTRACT)

A practical fiber optic strain sensor has been developed to measure strains in the range of 0.0 to 2.0 percent strain with a resolution ranging between 10 and 100 microstrain depending on sensor design choices. This intensity based sensor measures strain by monitoring strain induced longitudinal misalignment in a novel fiber interconnection. This interconnection is created by aligning fibers within a segment of hollow core fiber. Related splice loss mechanisms are investigated for their effect on resolution. The effect of gauge length and launch conditions are also investigated.

ACKNOWLEDGEMENTS

I wish to thank Dr. Richard O. Claus for serving as my advisor during my graduate studies at Virginia Tech and for introducing me to the stimulating field of fiber optics. I would also like to thank Doctors Gary S. Brown and Ronald J. Pieper for serving on my thesis committee.

I would next like to recognize Bernd D. Zimmermann for his formidable contribution to my work. The successful and timely completion of this work is due in no small part to the advice and encouragement of Mr. Zimmermann. Many thanks also go out to the other research associates of the Fiber and Electro-Optics Research Center: Russ May, Kent Murphy, Mike Gunther and Ashish Vangsarkar. Thank you also Linda Jones and Ann Goette and the student members of the center for your support towards the completion of this work. This research was sponsored in part by Lockheed Aeronautical Systems Company, Burbank, California.

This work is dedicated to the memory of my late father
Edmund Lathrop Andrews, Jr

TABLE OF CONTENTS

LIST OF ILLUSTRATIONS

1.0 INTRODUCTION.

The sensor to be presented in this thesis measures strain by detecting the strain-induced longitudinal misalignment of fibers within a fiber splice. The sensor offers the traditional advantages of fiber sensors including light weight, low profile, dielectric nature, high temperature capabilities, and immunity to many corrosive environments. A problem with many fiber sensors, however, is that they are difficult to use and may require prohibitively expensive equipment to operate. Further, many fiber sensor concepts are simply too expensive to be practical for many applications.

The sensor to be presented, alternately, offers excellent performance without many of these prohibitive factors. It is an easily mass producible sensor and offers the advantage of not needing to be individually calibrated. That is, one calibration curve will work for many different sensors. The sensor's sensitivity can also be easily tailored to match the needs of a particular application. Further, the sensor does not require expensive controlling electronics. It can be operated with simply a laser diode and an optical power meter. These issues will all be discussed in detail in the following pages.

This thesis will begin by discussing the motivation for this research. The motivation for fiber sensor research in general will be discussed as will

be the design considerations that motivated the development of this particular sensor. Next, the basic theory regarding the principle of operation of the sensor will be presented. Here the governing equations and expected results will be given. Following the discussion of theory will be a presentation of the sensor design and documentation of experimental work. Finally, a conclusion will summarize the work accomplished and give recommendations for future work.

2.0 MOTIVATION FOR THE RESEARCH.

The research and development of this sensor was motivated by a need to advance fiber sensing technology from a laboratory concept to a useful industry tool. Much research has been done in the development of optical sensing schemes for many applications but few actual "off the shelf" fiber sensors are available today. The research presented in this thesis hopes to move the field of fiber optic sensing one step closer to this end. Many approaches to strain sensing were considered but design considerations such as simplicity, mass producibility and cost quickly diminished this list.

Optical fiber sensors operate on the idea that some observable of interest will affect one of the fundamental propagation characteristics of light in an optical fiber. This disturbance in the light can then be interpreted to infer the change in the observable of interest. The fundamental propagation parameters of light travelling in an optical fiber are: time, amplitude, phase, modal distribution and polarization state. Sensors based on each of these parameters are called; time domain, intensity based, interferometric, modal domain and polarimetric sensors, respectively. While a clear distinction between the different sensor classifications is sometimes difficult to make, fiber optic sensors are generally devised so that some observable of interest, such as strain or

temperature, will change the value of one of these fundamental parameters. Beyond this general definition of fiber sensing, the sensing approaches can be extremely different.

Fiber sensors generally fall into two categories; extrinsic and intrinsic sensors. Extrinsic sensors are sensors for which the light exits the fiber, interacts with the environment and subsequently re-enters the fiber whereas intrinsic sensors keep the light within the fiber throughout. The sensor being reported in this thesis is in some ways a member of both of these classifications; again a fine line can exist between sensor classifications.

Time domain sensors are generally considered intrinsic sensors. These sensors operate on the principle that light pulses fired periodically into a fiber reflect off of imperfections in the fiber and return back toward the launch end of the fiber. These reflected pulses can then be detected at the launch end or reflected again for transmissive mode time domain sensing. It is the arrival time of these pulses that provides the useful information about the fiber. For example, this technique is used to measure strain by monitoring the increase in delay time of a pulse that is reflected from the far end of a fiber that has been elongated by strain. It is the time delay that gives us the information about strain, hence the classification time domain sensor.[1] Time domain sensors can also be used with more elaborate techniques for temperature sensing, shape sensing and more.

Intensity based sensors use effects on loss mechanisms in fibers to infer useful information about the environment. Loss mechanisms such as microbending, macrobending and splice loss have been researched as sensing approaches.[2] [3] These sensing approaches generally offer the advantage of simplicity and cost but generally a trade off is made with sensitivity. Problems such as source drift and micro and macro bending on the lead-in and lead-out fibers also tend to decrease resolution. For applications where these effects can be controlled or where tremendous sensitivity is not needed these sensors offer a great deal in the interest of practicality.

Interferometric sensing is a method where a signal is split and the two parts transmitted down two different paths where one signal interacts with the environment and one does not. The two signals are then reunited where an interference pattern results. It is this changing interference pattern that will yield the useful information about the observable of interest. Because the wavelength of light is so small, extremely small changes in the optical path length or refractive index will affect the arrival time of the perturbed signal appreciably so that a change in the interference pattern is detected. Thus, these sensors are very sensitive. Interferometric sensors are used mostly for applications where extremely high sensitivity is required. These applications would include acoustic emission detection, ultrasonics, and magnetic field sensing. Interferometric sensors, while having high sensitivity, also have drawbacks. For many applications they are simply too sensitive. Further, single mode fiber must be used and for many applications it

must be polarization maintaining fiber which can be prohibitively expensive. For many applications, however, these sensors are very effective.

Modal domain sensing is a relatively new sensing approach where the modal distribution in a fiber is monitored to infer useful information about the environment. Perturbations to fibers such as micro and macro bending will change the modal distribution in a fiber. This effect can be monitored through the use of spatial filters as the light exits the fiber. These sensors offer a sensitivity approaching that of interferometric sensors and thus have some of the same trade-offs.

Polarimetric sensors operate on the principle that fiber perturbations alter the polarization state of a mode in a single mode fiber. This can be accomplished by launching light through a linear polarizer into the fiber and then detecting it at the other end through another polarizer. The degree to which this the polarization state is changed is then indicative of the magnitude of the perturbation.

Each of the above sensing techniques has at one time been used to detect strain. The sensor being reported in this thesis falls somewhere near the lower end of the sensitivity spectrum but in exchange is very inexpensive to fabricate and operate and thus is very practical. The question then arises, "how does it compete with conventional strain gauges?".

Most strain gauges used in industry today are of the electric foil type. That is, a piece of metal foil has a resistance that is a function of strain. Therefore for this sensor the voltage drop across the sensor is monitored to infer the applied strain. These sensors generally have a sensitivity of a few microstrain. They have been widely used for years and thus offer the advantage of reliability and relatively low cost. These sensors are not, however, without problems. For many applications this type of sensor cannot be used. Because these sensors are electric in nature they are subject to electromagnetic interference from co-located electronic equipment. The metallic nature of these sensors also causes them to act as a thermal conduit to or from the sensing region. For high temperature applications this is certainly a hinderence. Further there output value is a function of the ambient temperature. As is shown in Figure 2-1, the ambient temperature in the sensing region must be either stable or monitored continuously for accurate operation.[4] Each and every one of these problems is overcome by the fiber optic sensor presented in this thesis. In the following chapters the details of this longitudinal misalignment based strain sensor are reported in detail.

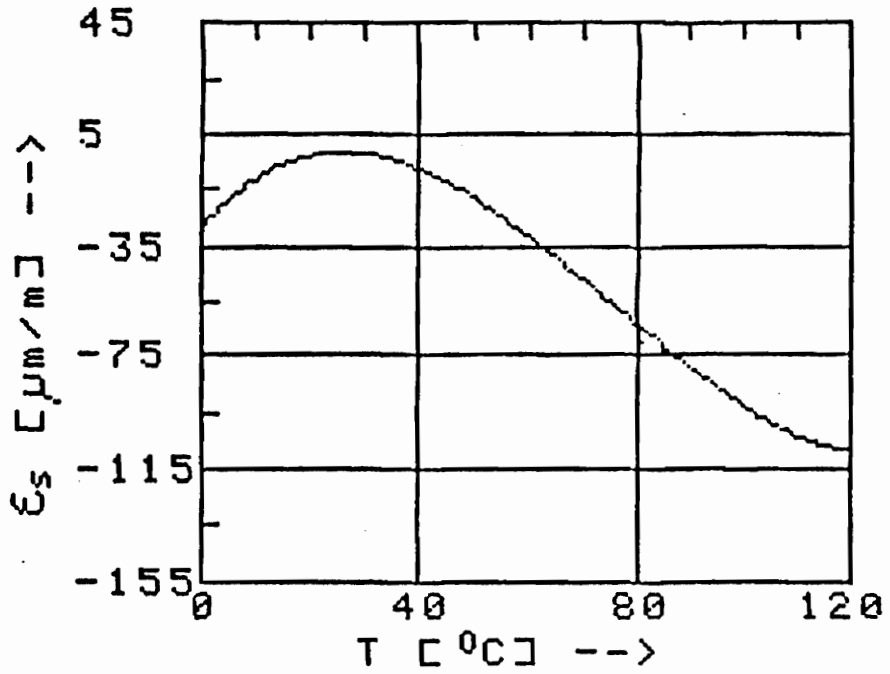

Figure 2-1. Temperature dependence of electric foil strain gauges. T is temperature and ε is strain.

3.0 THEORY.

Many loss mechanisms exist in fiber interconnections. These mechanisms generally fall into two categories, extrinsic and intrinsic losses. Extrinsic losses are due to longitudinal misalignment, lateral misalignment and angular misalignment of the fiber ends. Intrinsic losses are losses due to the propagation characteristics of the two fibers being joined.[5] These would include losses induced by changing modal distributions and differences in the waveguide parameters of the lead in and lead out fibers. The most critical of these waveguide parameters are the core diameter, numerical aperture, and index profile of the two fibers. Because the lead in and lead out fibers are assumed identical in the sensor being discussed, the effects of parameter mismatch are not present. Other intrinsic losses include mode stripping effects and micro and macro bending losses caused by distortion of the waveguide. In the case of the fiber sensor being reported, leaky modes are stripped by a lossy fiber jacket.[6] Effects due to different modal distributions in the core however, will be investigated for their possible effect on sensitivity. Loss caused by distortion of the waveguide is considered intrinsic because its *magnitude* is dependent on the above waveguide parameters. All of these issues will be discussed in detail in the following sections. The extrinsic loss mechanisms will be addressed first followed by the

intrinsic mechanisms. The equations for graded index fibers become somewhat complex as variables are changed and normalized. Therefore refer to Figure 3-1 for aid in interpreting these variables. The most important parameters to understand in figure 3-1a are the longitudinal misalignment, s, the lateral misalignment, u, and the angular misalignment, θ. In figure 3-1b (r,ψ) are the position polar coordinates on the recieving fiber and (θ,ϕ) the angular polar coordinates on the recieving fiber. For the equations pertaining to graded index fibers the primed system is the coordinate system of the emitting fiber and the unprimed system that of the recieving fiber.

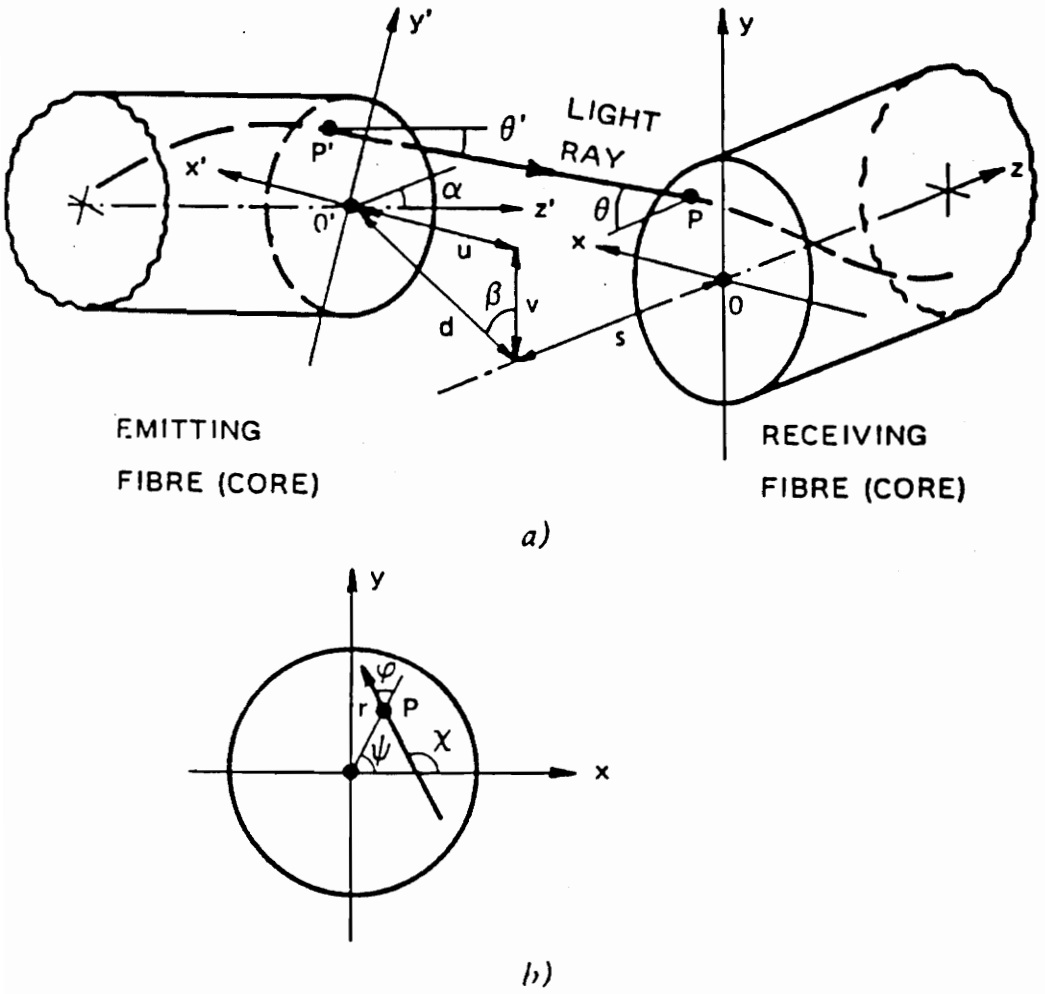

Figure 3-1. Fiber misalignment parameters [7]

3.1 Longitudinal Misalignment.

Longitudinal misalignment is the misalignment of fibers in the fiber axis direction. Equation (3.1) describes the power transmitted to a longitudinally misaligned graded index fiber assuming all modes are equally excited and all cladding modes stripped.[8]

$$W = \frac{2\pi R_o}{n^2}\int_0^{\cdot} r\,dr \int_0^{\pi} A^2\left[r(r,\phi),\phi\right]d\phi \qquad (3.1)$$

R_0 is the radiance distribution in the plane containing the endface of the emitting fiber and $A(r,\phi)$ the local numerical aperture of the lead out fiber for a given value of r and ϕ. This equation is integrated over the recieving fiber cross section. Figure 3-2 illustrates this idea of local numerical aperture. The numerical aperture of a fiber is defined as the sine of the half angle of the cone of acceptance of the fiber. It is determined by the index profile and geometry of the fiber.

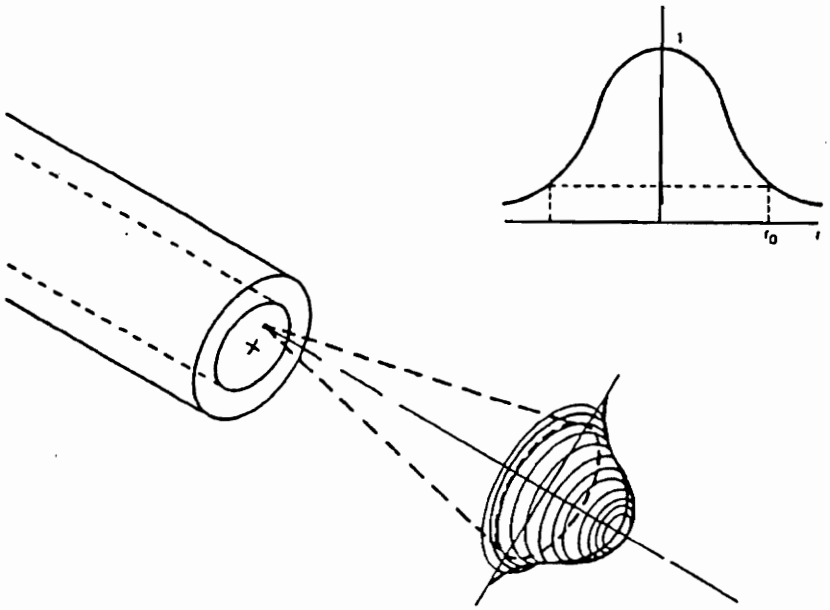

Figure 3-2. Illustration of local numerical aperture [9]

Each point on the endface of the launch fiber is treated as an individual light source that creates a certain radiance distribution on the receiving fiber. n' is the index of the splice region separating the fiber ends. Further, the formulation of this equation assumes that the lead in and lead out fibers are identical. $\bar{r}$ is defined as follows: [10]

$$\bar{r} = \left\{ \begin{array}{l} r : A^2(r,\phi) < A^2(r',\phi) \\ r' : A^2(r,\phi) > A^2(r',\phi) \end{array} \right\} \qquad (3.2)$$

where r' is defined implicitly by:

$$1 + s^2\left[r'^2 + r^2\cos 2\phi - 2r\cos\phi\left(r'^2 - r^2\sin^2\phi\right)^{1/2}\right]^{-1} = \frac{n'^2}{A^2(r',\phi)} \qquad (3.3)$$

where s is longitudinal misalignment. Figure 3-3 shows theoretical plots of constant coupling efficiency (P/Po) for graded index fiber as longitudinal and lateral misalignment are varied. $\bar{s}$ and $\bar{u}$ are the longitudinal and lateral misalignment parameters normalized to one core radius. To infer longitudinal misalignment alone we select one value of lateral misalignment (zero) and interpret the longitudinal loss vs. coupling efficiency along this line. This plot is generated by a computer using the above equations describing longitudinal misalignment and the equations for lateral misalignment described in the next section.

Equation (3.4) describes the splice loss due to longitudinal misalignment for step index fibers assuming all modes are equally excited and all cladding modes are stripped.[11]

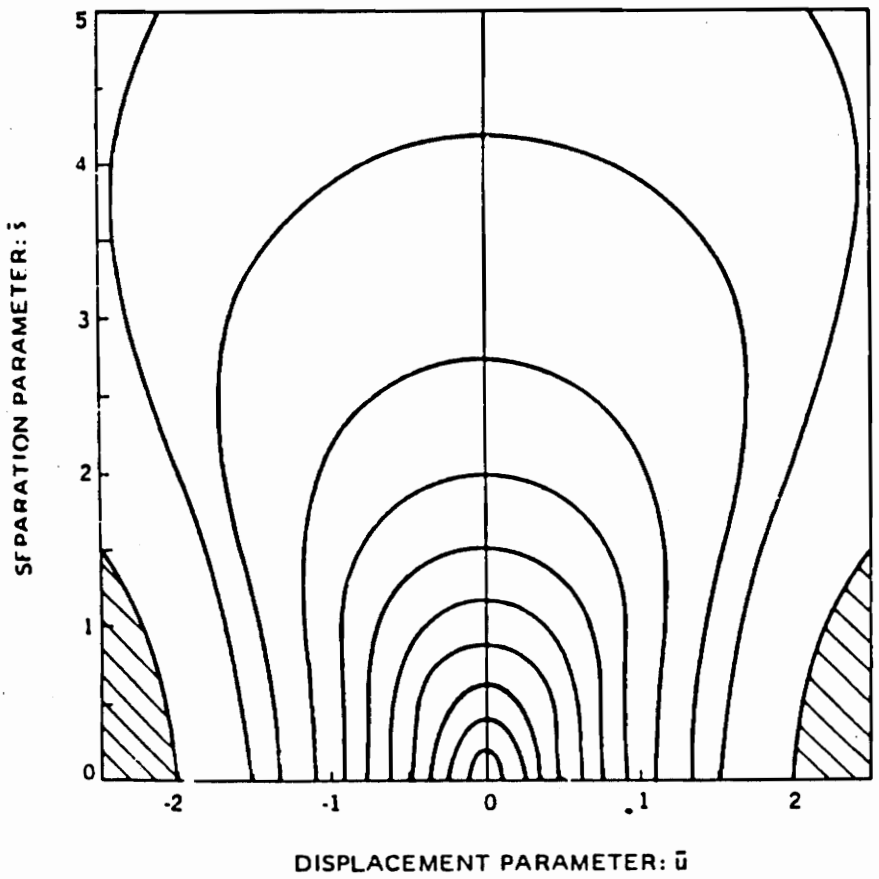

Figure 3-3. Curves of constant coupling efficiency. P/Po = 0.05, 0.1, 0.2, 0.3, 0.4, 0.5, 0.6, 0.7, 0.8, 0.9. [12]

$$\frac{P}{Po} = \left[\frac{r}{r + S\tan\left(\sin^{-1}\left(\frac{NA}{n_o}\right)\right)} \right]^2 \qquad (3.4)$$

S is the longitudinal misalignment, r the core radius, n_0 the index of the splice region and NA the numerical aperture of the two fibers (assumed identical). All of the equations for step index fiber misalignment are derived using a simple geometrical approach under the above assumption that the core is uniformally illuminated.

The plot of longitudinal misalignment vs. coupling efficiency(P/Po) for both graded and step index is shown in Figure 3-4. The error bars for the graded index plot are associated with error in reading the plots in Figure 3-3.

As one can see in Figure 3-4, the theoretically predicted change in loss due to a given amount of longitudinal misalignment is different for these two types of fiber. This fact will be an advantage in tailoring the sensor to a specific application.

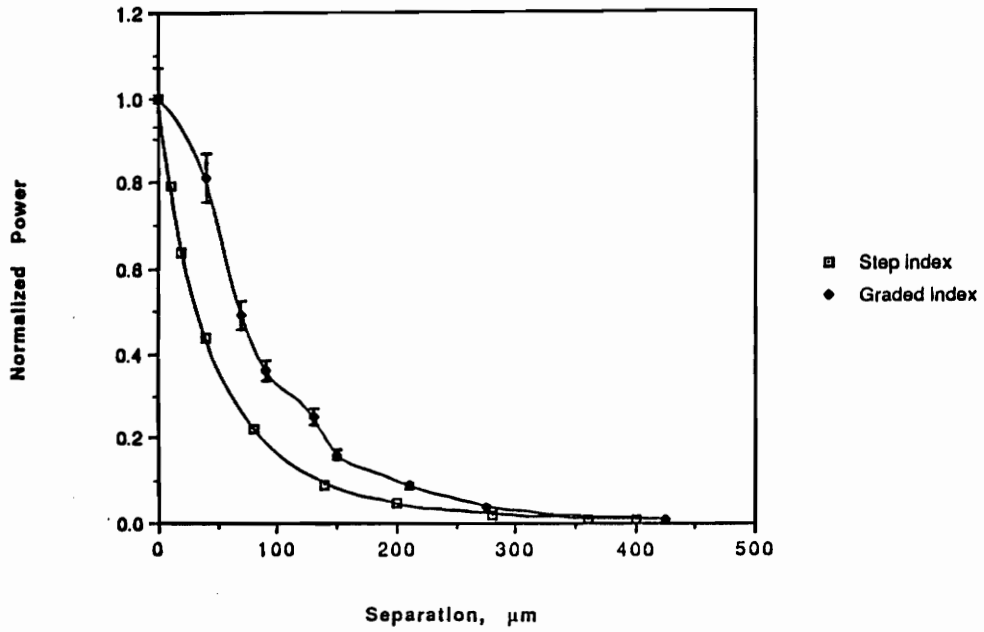

Figure 3-4. Theoretical longitudinal misalignment loss

3.2 Lateral Misalignment.

Lateral Misalignment is the offset of fibers in the direction transverse to the direction of propagation. It is the largest single extrinsic source of splice loss. For the sensor being reported, however, it is a controllable factor. This factor is controllable because the hollow core fiber keeps the two sensor fiber endfaces aligned to within a few microns. In addition, it is found through experiment that the transverse mismatch stays relatively constant during operation further minimizing any standard deviation from this effect.

Equation (3.5) describes the loss induced by lateral misalignment of graded index fiber.[13]

$$W = \frac{2\pi R_o}{n^2}\int_0^{*} r\,dr \int_0^{*} A^2\left[\bar{r}(r,\psi),\psi\right]d\psi \qquad (3.5)$$

$A(r,\psi)$, r, and R_o have the same meanings as stated above. The integration, however, is now performed over ψ. ψ is the angular coordinate with respect to the particular point on the fiber endface (see Figure 3-1). Further r' is now defined as:[14]

$$r' = \left(r^2 + d^2 + 2rd\cos\psi\right)^{1/2} \qquad (3.6)$$

Equation (3.7) describes the loss induced by lateral misalignment of step index fibers.[15]

$$\frac{P}{P_o} = 1 - \frac{2}{\pi}\frac{d}{2a}\left[1 - \left(\frac{d}{2a}\right)^2\right]^{1/2} - \frac{2}{\pi}\sin^{-1}\frac{d}{2a} \qquad (3.7)$$

Again a strictly geometrical approach is used in this derivation. a is the core radius, d the lateral misalignment and ψ the local angular coordinate. Figure 3-5 shows the curves for the theoretically predicted losses due to lateral misalignment for graded and step index fibers. It should be noted that these curves describe losses incurred when operating in the reflective mode. Operating in the reflective mode offers the advantage of increased sensitivity because the signal traverses the splice region twice, hence the power is attenuated faster for a given amount of lateral offset.

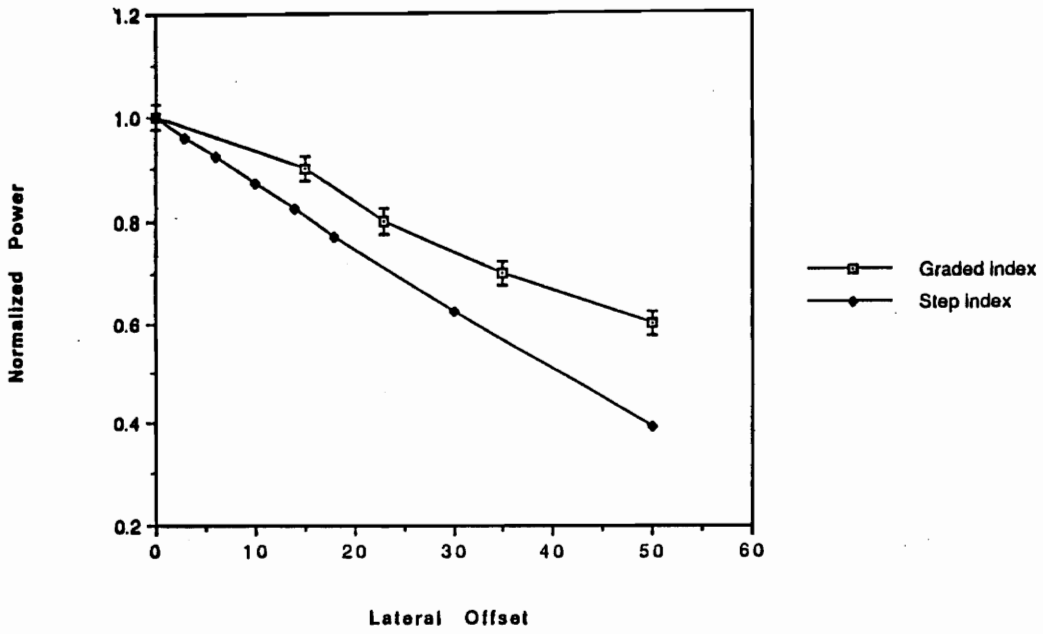

Figure 3-5. Theoretical misalignment loss

3.3 Angular Misalignment.

Angular misalignment is the misalignment of fibers where the axes of the fibers are not colinear but rather form an angle, θ. Angular misalignment is an effect that cannot occur by itself. That is, a gap of some kind between adjacent portions of the endfaces must also be present as shown in Figure 3-6.

While this effect is not as significant as the lateral misalignment loss, it can be a sizable source of loss in some applications. The loss due to angular misalignment for graded index fibers is defined by: [16]

$$W = \frac{2\pi R_o}{n^2} \int_0^a r\,dr \int_{-\pi/2}^{\pi/2} \left[A^2{}_2(r,\chi) - A^2{}_1(r,\chi) \right] d\chi \qquad (3.8)$$

The parameters here are the same as discussed above but A_1 and A_2 refer to the local numerical apertures of the transmitting and receiving fibers, respectively. The loss due to angular misalignment for step index fibers is defined by:

$$\frac{P}{Po} = \cos\theta \left\{ \frac{1}{2} - \frac{1}{\pi}\rho\left(1 - \rho^2\right)^{1/2} - \frac{1}{\pi}(\sin\rho)^{-1} + q\left[\frac{1}{\pi} r\left(1 - r^2\right)^{1/2} + \frac{1}{\pi}(\sin r)^{-1} + \frac{1}{2} \right] \right\}$$

where

$$\rho = \frac{\cos\theta_c(1 - \cos\theta)}{\sin\theta_c \sin\theta}$$

$$q = \frac{(\cos\theta_c)^3}{\left((\cos\theta_c)^2 - (\sin\theta)^2\right)^{3/2}}$$

$$r = \frac{(\cos\theta_c)^2(1 - \cos\theta) - (\sin\theta)^2}{\sin\theta_c \cos\theta_c \sin\theta}$$

$$\theta_c = \left(\sin\left(\frac{NA}{n}\right)\right)^{-1}$$

(3.9)

Figures 3-7 and 3-8 show the loss due to angular misalignment for graded and step index fibers. This equation is derived using a strictly geometric approach for the intersection of the two cones defined by the fiber numerical apertures.

Due to the design of the sensor being reported, angular misalignment is not anticipated to be a problem and thus no further work is planned to document its characteristics.

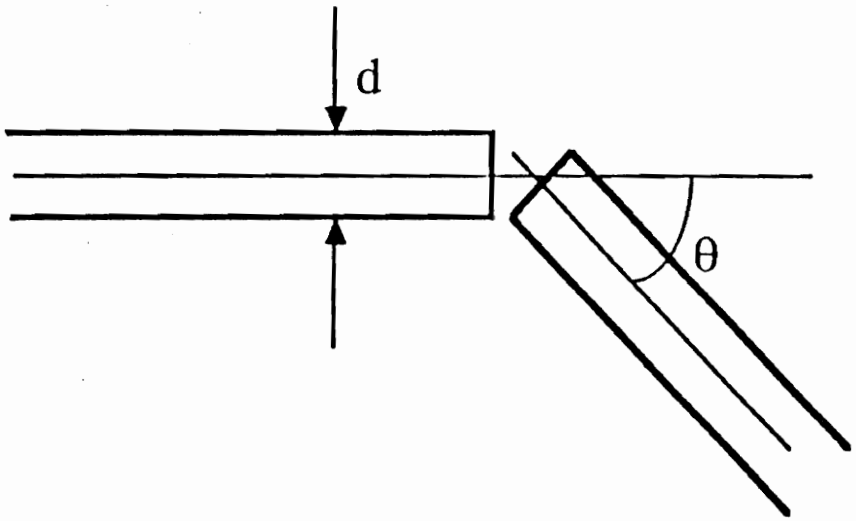

Figure 3-6. Illustration of angular misalignment

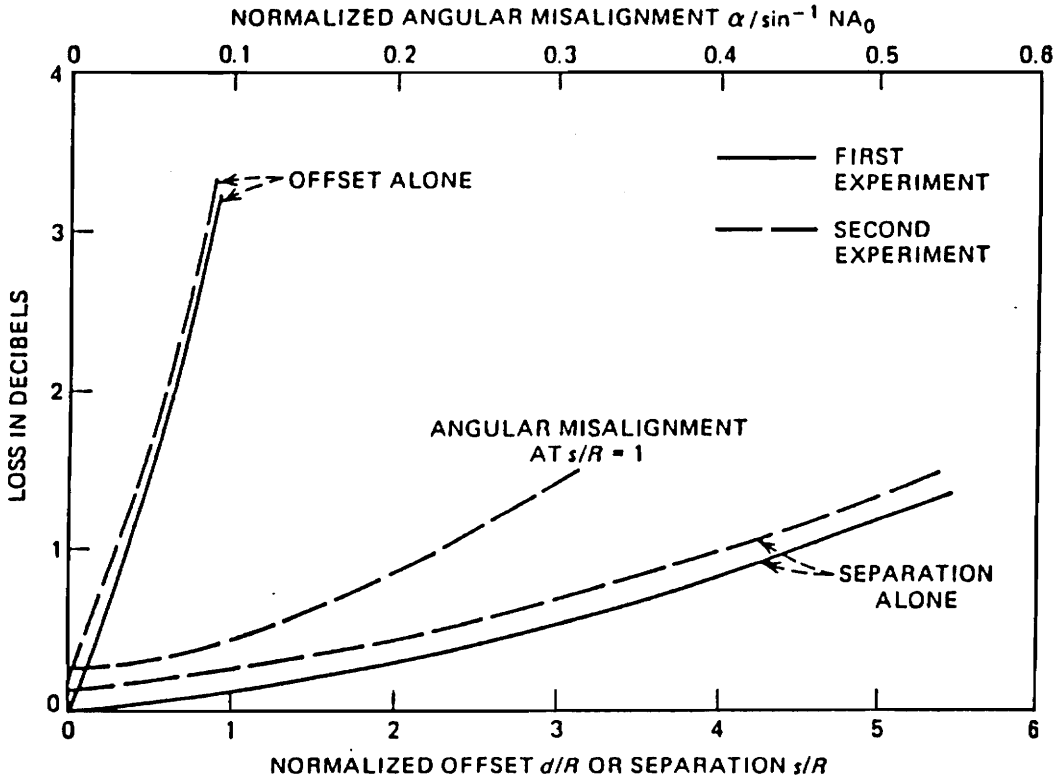

Figure 3-7. Angular misalignment loss; graded index. R is fiber core radius. [17]

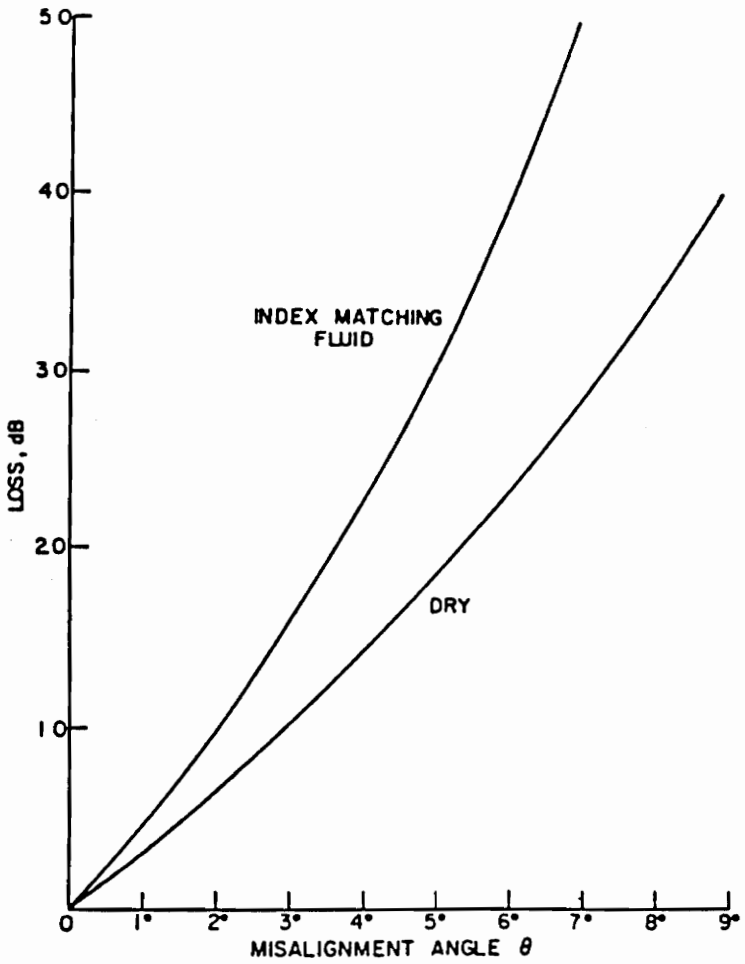

Figure 3-8. Angular misalignment loss; step index [18]

3.4 Launch Condition Effects.

Because the sensor is fabricated with multimode fiber, it is anticipated that modal distribution may have a significant effect on the performance of the proposed sensor. For this reason a brief review of multimode fiber theory will be presented highlighting issues that are of interest in the development of the sensor.

Glass fibers are able to guide light because of the elevated refractive index of the core region over that of the cladding. Having met this requirement certain critical parameters become important. The first parameter of interest is the difference in index between the core and cladding regions. This difference is made very small in order to minimize inter-modal dispersion in multimode fibers and to retain manageable core sizes in single mode fibers. Further, the index difference affects the total number of modes that can propagate in the fiber. Our primary interest is its effect on the number of modes propagating. The number of modes is also frequency dependent and thus the light source is a critical element in determining the number of modes that can propagate. Finally, the core size will affect the number of modes. The total number of modes for large values of V is: [19]

$$\text{Total Number of Modes} = 4V^2 / \pi^2. \qquad (3.10)$$

Where V is the normalized frequency and is defined by [20]

$$V^2 = (n_1^2 - n_2^2)ka \qquad (3.11)$$

Note that as the index difference, $(n_1 - n_2)$, increases so does the number of modes. Similarly, higher frequencies and larger core radii increase the number of modes that can propagate. Figure 3-9 shows the normalized frequency V vs. the normalized propagation constant b. Each line in this figure represents the behavior of a distinct mode. The intersection of each line with the horizontal axis defines its cutoff frequency or frequency below which the mode will not be supported by the waveguide structure.

At a given operating frequency each mode has a unique propagation constant ß = nk. n is the refractive index and k the plane wave propagation constant in free space. b is simply equal to b = ß/k. For a mode to be guided ß must lie in the interval:

$$n_2k < ß < n_1k. \qquad (3.12)$$

Because the core of a multimode fiber is so large compared with the wavelength of light, a ray optics model can be used to understand the difference between

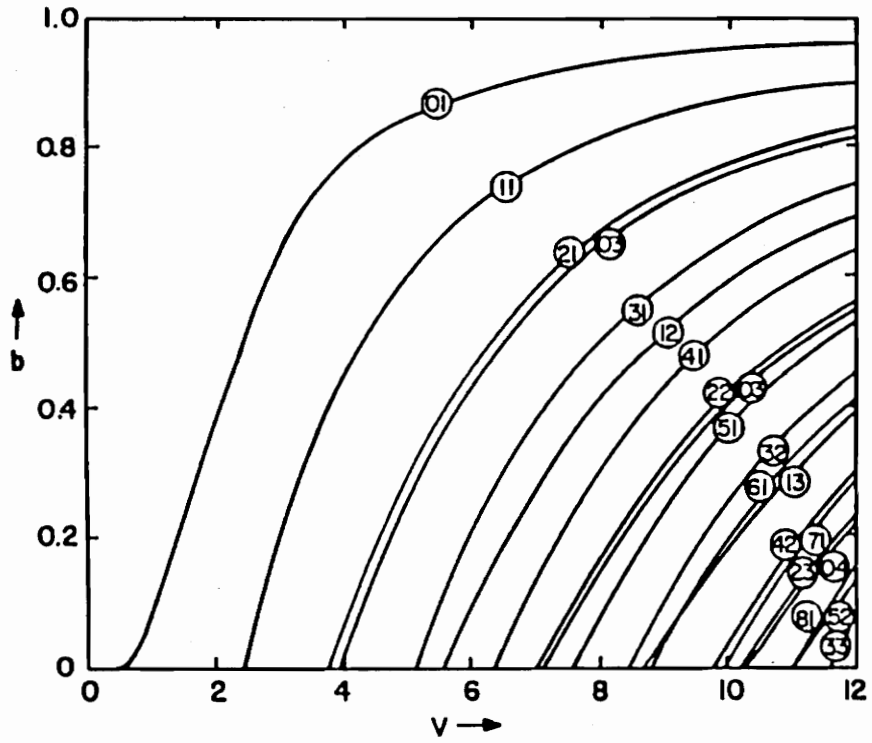

Figure 3-9. Normalized dispersion curves [21]

higher and lower order modes. Using this ray optics model, the angle of incidence of a mode increases toward the critical angle of the fiber as ß approaches n_2k. Because the higher order modes propagate at higher angles they are on the outside edge of the exit light cone defined by the numerical aperture when the light exits the fiber. For this reason it is anticipated that these modes will be the first to be lost when the receiving fiber is misaligned in the longitudinal direction. Hence, when a large number of higher modes are excited the strain sensor being presented is expected to be more sensitive whereas a launch that excites only low order modes, that stay relatively close to the fiber axis, is expected to make the sensor less sensitive. This effect will be investigated in the experiments.

3.5 Gauge Length.

As modal distribution affects sensitivity of this sensor so does the gauge length. Recall in chapter 1 that the fibers within the hollow core fiber have an initial gap S_0. The change in fiber separation, however, is determined by the degree to which the *hollow core fiber* is strained. Recall the hollow core fiber has an initial length L_0 and when strained elongates to some length $L_0 + dL$. Thus the fiber separation within the hollow core fiber becomes $S_0 + dL$. The sensitivity of the sensor is then dictated by the magnitude of dL for a given amount of strain. This is a function of the zero strain length of the hollow core fiber or gauge length. 1 percent strain on a 1cm section of hollow core fiber translates to dL = $(.01)(1x10^{-2}m)$ = 100 microns. Thus the fiber separation within the hollow core fiber segment increases by 100 microns. This clearly falls into the range of operation of the sensor. If an application required measurements over a region of 0 to 0.1 percent strain then a sensor of gauge length 10cm would deliver the same resolution as did the 1cm sensor over an operating range of 1.0 percent strain. In effect, the sensitivity of the sensor can thus be tailored to a specific operating range for a given application. The effects of gauge length on sensitivity will be investigated in the experiments.

4.0 SENSOR DESIGN.

Many factors contributed to the design of this sensor. When the research was initiated what was needed was a sensor that was effective in detecting strain. Many other design considerations, however, factored in to the final concept presented in this thesis. These additional design considerations include mass producibility, cost of fabrication, cost of the operating system as well as load range and sensitivity. Several novel sensing concepts were eliminated for failing to meet one or more of these requirements.

The sensor is depicted in Figure 4-1. It is created by inserting two fibers into opposite ends of a section of hollow core fiber. The fibers are then bonded to the ends of the hollow core fiber by packaging the insertion point of the lead-in fiber into the hollow core within a short section of stainless steel capillary tubes and then filling this region with epoxy. This is repeated at the opposite end of the hollow core fiber segment leaving an effective gauge length equal to the distance between the two stainless steel capillary tubes. It will be shown in Chapter 5 that the

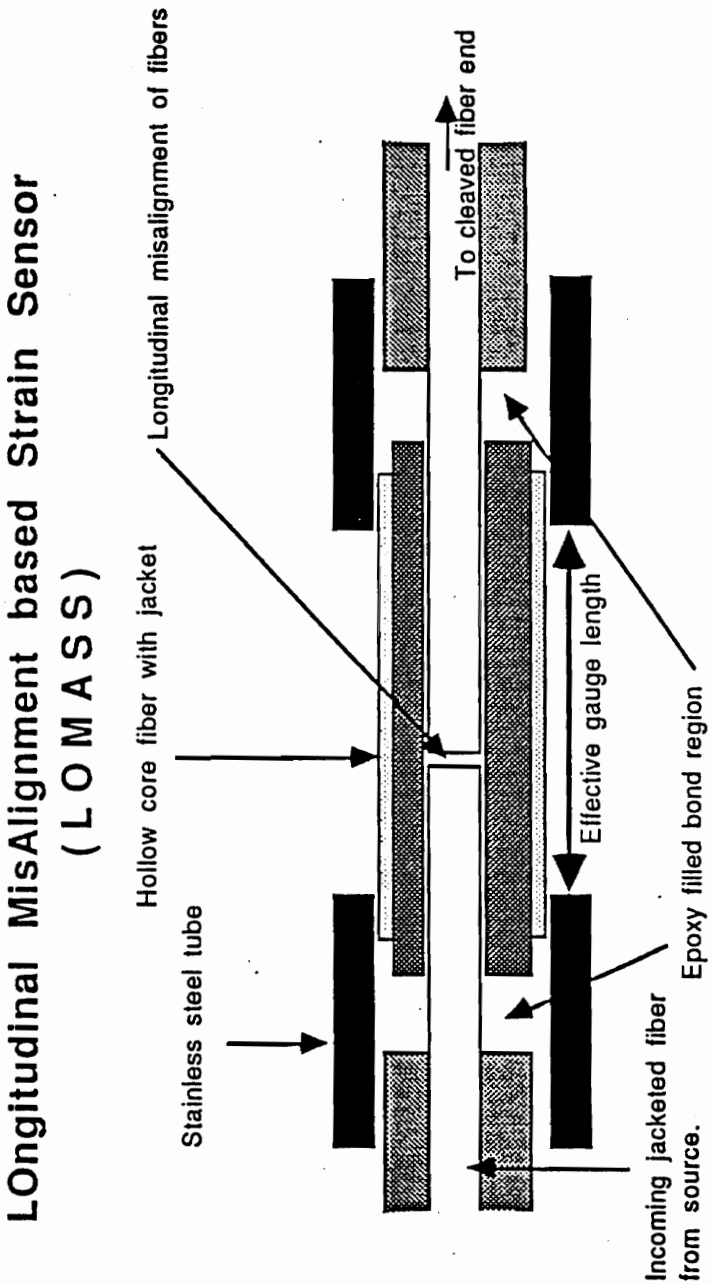

Figure 4-1. Sensor Design

initial gap between the fiber ends within the hollow core fiber is a key variable in sensor performance. Therefore the sensor is fabricated under a microscope where this gap can be monitored. It will be demonstrated in Chapter 5 that this gap does need to be within a certain window of acceptance but that this window is large with respect to the alignment resolution and therefore initial gap variation is not a problem. Figures 4-2 shows magnified pictures of this initial gap between the fiber tips. Figure 4-2a is a picture of sensor created using 100/140 fiber and a gauge length of 3.9cm. Figure 4-2b depicts a sensor made of 50/125 fiber and as can be seen in the figure has a near zero initial gap. As will be demonstrated in chapter 5 this small initial gap will affect the sensor performance.

Another issue that needed to be addressed is what type of fiber to use. The choices are somewhat limited by the hollow core fiber. That is, currently only two sizes of hollow core fiber are available at the Fiber and Electro-Optics Research Center (FEORC). This specialty fiber is manufactured at FEORC's fiber fabrication facility. The two sizes are 145 micron and 127 micron inner diameter hollow core. This is limiting because the fibers to be inserted must then have outer cladding diameters of 140 and 125 microns, respectively, on order for lateral misalignment losses to be acceptable. Experiments will be reported in Chapter 5 that document the effect of fiber choice on sensor performance.

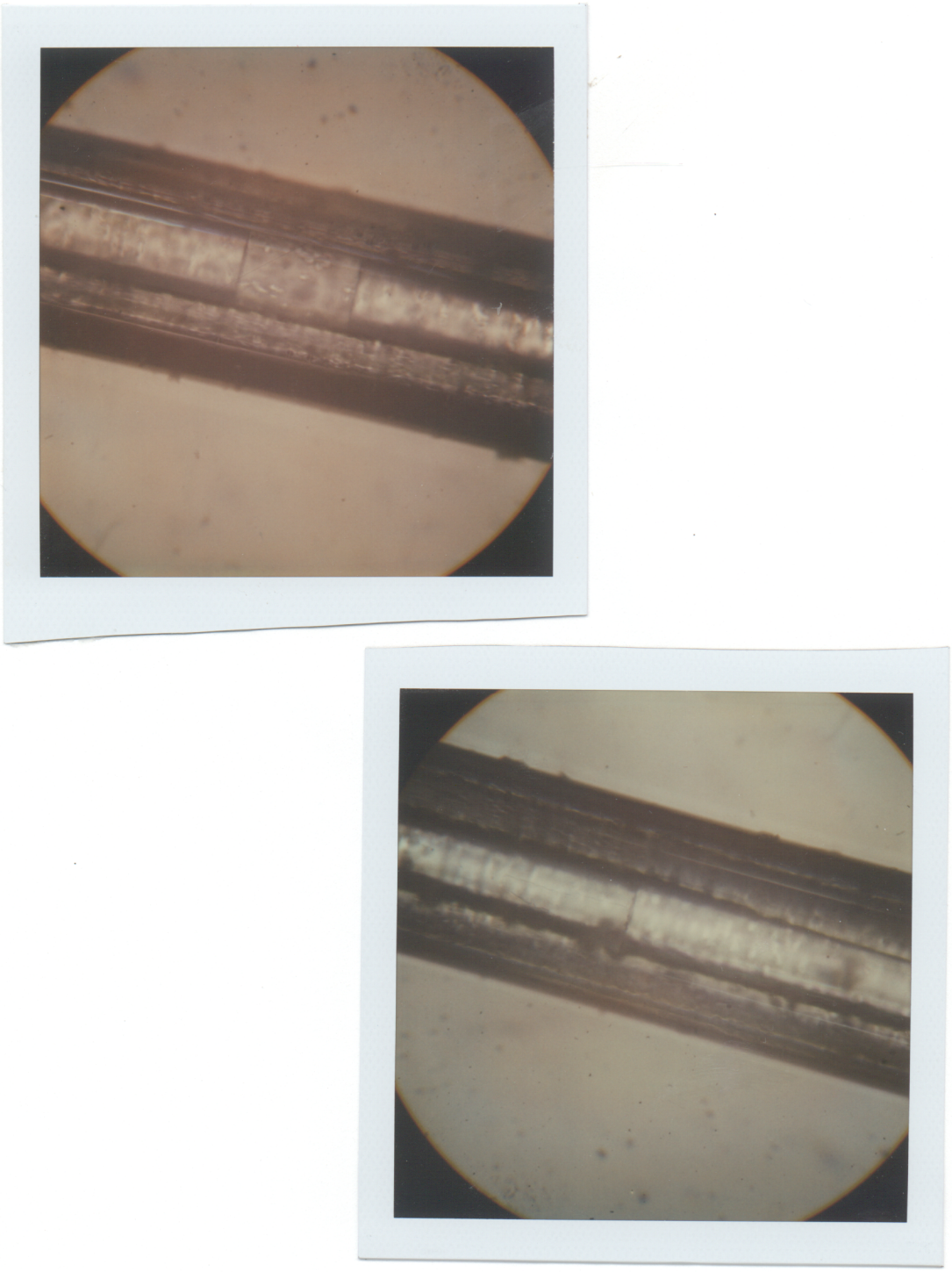

Figure 4-2. Initial gap photographs

Two of the critical design parameters for this sensor were cost and mass producibility. This design meets both of these constraints. The sensor can be fabricated in approximately one hour using commercially available fiber and the hollow core fiber manufactured at FEORC. For external tensile loading the aforementioned design using the stainless steel capillary tubes at the hollow core fiber ends would be used. For embedded composite applications, however, the steel capillaries are not necessary. For this application the composite material will serve to bond the fibers to the hollow core. The fibers would be inserted into the hollow core fiber and simply tacked into place with a single drop of epoxy. This epoxy would serve only to maintain the initial fiber gap while the sensor is laid into the composite.

A further advantage of this sensor design is the cost of the operating electronics. If the highest sensitivity is needed an optical time domain reflectometry (OTDR) system will be necessary but if sensitivity does not need to be optimized the sensor can be operated in the transmissive mode with simply an LED and optical power meter. Clearly the cost of the operating electronics is relatively small compared to other strain sensing concepts. All of these design considerations inspired the development of this sensor concept. An inexpensive, mass producible, effective strain sensor was the result.

5.0 EXPERIMENT.

Many of the technical questions posed in Chapter 3 will now be investigated experimentally. The first experiment to be performed was one to verify that loss due to longitudinal misalignment is a significant effect and of sufficient magnitude to be used in strain sensing. This was accomplished by measuring splice loss as a function of controlled longitudinal separation on an alignment stage. Once the basic concept was confirmed to be a promising approach to strain sensing, a prototype sensor was fabricated and tested. This prototype sensor proved to be very effective at measuring strain. These results then initiated further supporting experiments.

Subsequent experiments documented the effects of many factors that contribute to overall sensor performance. These issues include: waveguidance by the hollow core fiber, lateral misalignment of the fibers within the hollow core fiber, the effect of sensor gauge length on sensitivity, the effects of different fiber geometries and the effect of changing launch conditions on sensitivity. Each of these experiments is discussed below.

5.1 Longitudinal misalignment as a sensor concept.

Longitudinal misalignment experiments were performed by simply aligning the incoming and outgoing fibers on an alignment stage until maximum power was transferred signifying that the transverse alignment was optimal. The outgoing fiber was then backed off in increments as power readings were recorded. This was done with and without the hollow core fiber present in order to document what waveguiding ability, if any, the hollow core fiber exhibited. The results are illustrated in Figure 5-1. They are expressed in terms of normalized power.

It is interesting to note that the transmitted power levels taken with the hollow core fiber present are slightly higher than those taken without. It appears that the hollow core fiber does exhibit some wave guiding properties. Error bars are present on this graph for the experimental plots but are very small.

It is also clear that measured results are very different from the theoretically predicted results. It is the opinion of several researchers that the discrepancy between experiment and theory is due primarily to the assumption of full and equal modal excitation.[22] [23]

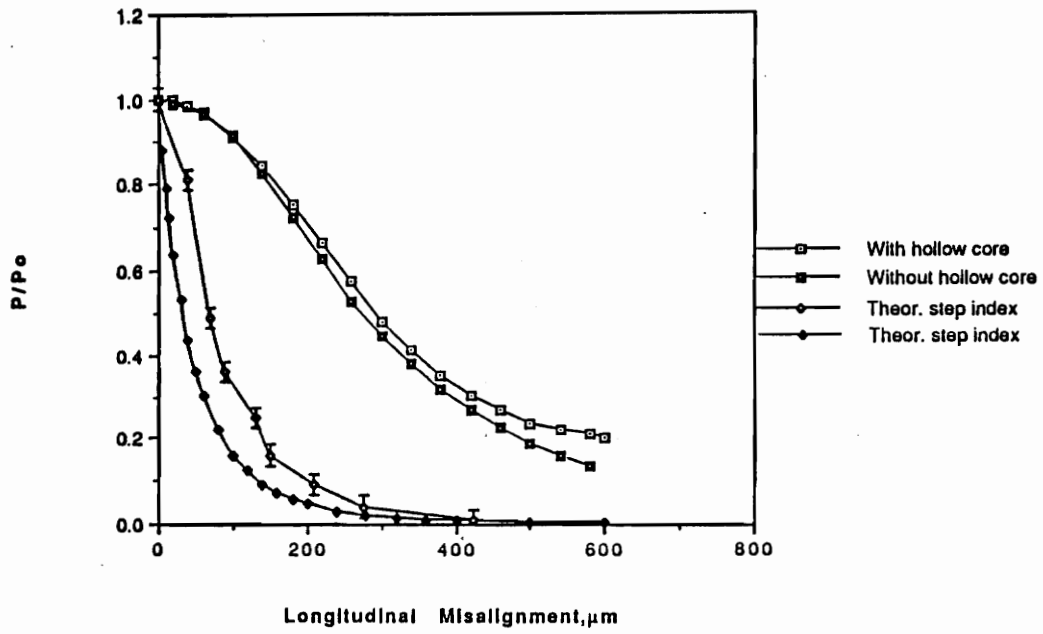

Figure 5-1. Longitudinal separation vs. normalized power

Notice the relatively large range of linear behavior in the experimental results. This is significant because the linear range is relatively long, corresponding to approximately 300 microns of fiber movement. As will be discussed later, this can represent a wide range of strain levels depending on the gauge length of the sensor. Further, if one could "set" the initial unstrained fiber separation so the sensor operates only in the linear region, an exclusively linear relationship will exist between strain and normalized power. Assuming that the initial fiber separation is an easily adjusted parameter, it appears that once the slope of the calibration curve is known, any sensor with an initial gap within the tolerance region will be able to use the same calibration curve.

5.2 Prototype Sensor Characterization.

Having established that the sensor concept was effective for detecting longitudinal separation, a prototype sensor was fabricated. The sensor was assembled as in Figure 4-1. The sensor was fabricated from Spectran 100/140 graded index fiber. The hollow core fiber was approximately 145 micron inner diameter and 205 micron outer diameter. The effective gauge length of the sensor was 10.8cm and the initial gap between the fibers within the hollow core segment was 210 microns. The stainless steel capillary tubes used to strain relief the fiber/hollow core interface were filled with Tra-Con BA-F113SC epoxy. The the sensor characterization apparatus was assembled as in Figure 5-2. The system was incrementally loaded with weights up to approximately 700 grams. Only one half of that mass is actually supported by the sensing region. Between each loading a zero strain value was recorded to verify the sensor's integrity and to detect any hysterisis. When the normalized power value P/Po is calculated, this zero value and its associated standard deviation are used. This gives a more realistic representation of the sensor's resolution.

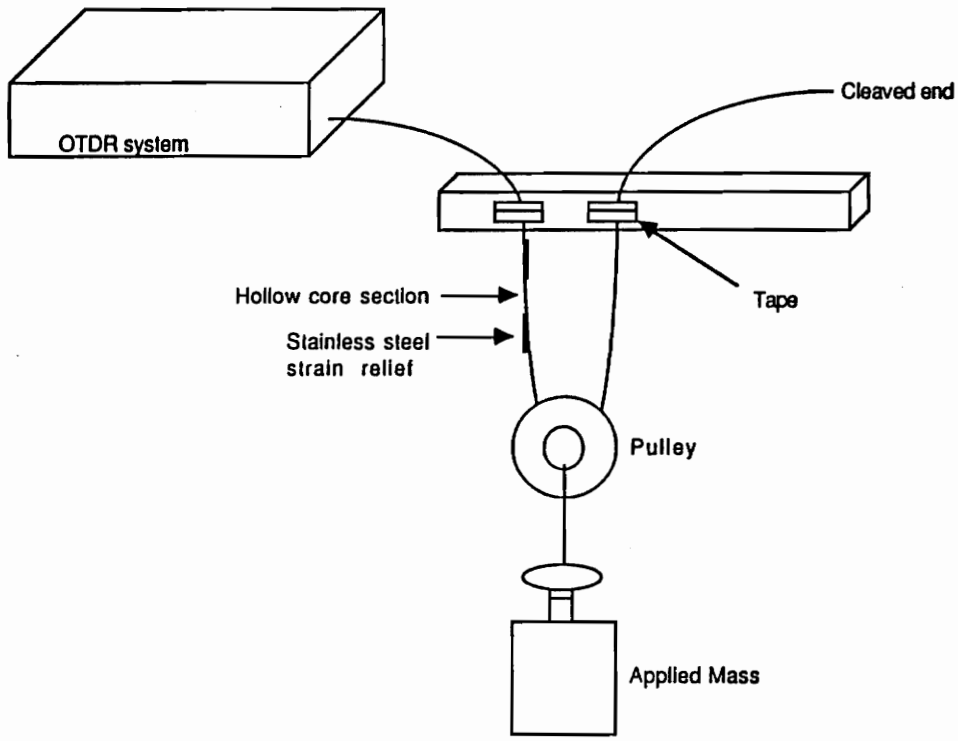

Figure 5-2. Experimental test set-up

Because fused silica exhibits nearly linear elongation under tensile loading it is expected that applied mass will be in direct proportion to change in fiber separation. Therefore a curve similar in shape to that in Figure 5-1 is expected for applied mass vs. normalized power. We see these results in Figure 5-3.

It is clear that the sensor is effective in detecting strain. The results also agree reasonably well with the predicted results from section 5.1. The strain level in the fiber for the applied mass of 350 grams is approximately 0.1 percent. Thus the sensor is rather sensitive when it has a gauge length on the order of 10cm. The affect of gauge length on sensitivity will be further investigated in subsequent sections.

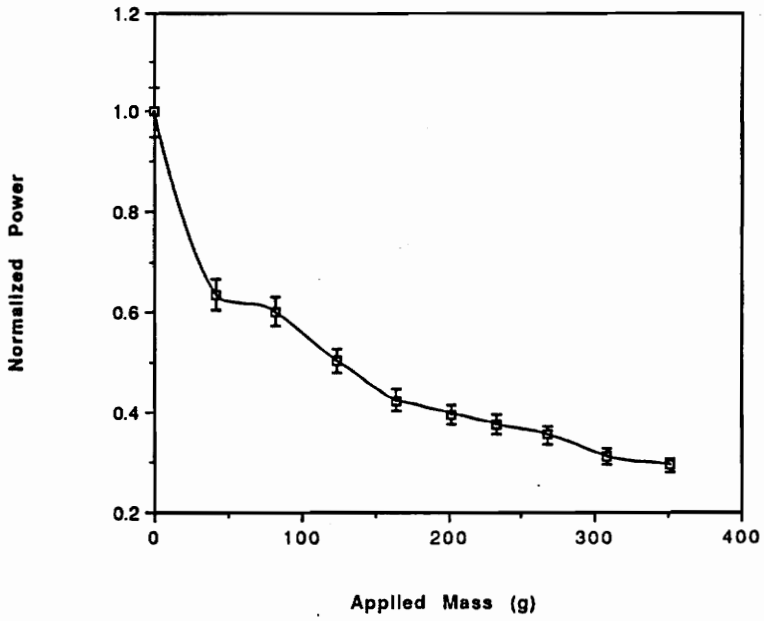

Figure 5-3. Applied mass vs. power; prototype sensor

5.3 Affect of Core Diameter on Sensitivity.

Having demonstrated that the sensor works as predicted, many questions arise as to what variables in the sensor design will affect sensitivity. The first parameter to be investigated is core diameter. The principle of operation of this sensor dictates that the affect on splice loss from a given amount of longitudinal separation should vary with different core sizes. That is, a 30 micron gap between two fibers with 100 micron diameter cores will not suffer the same loss as a 30 micron gap between fibers with 4 micron cores. It would seem reasonable that the 4 micron core fibers would suffer a greater loss. This, however, is not necessarily the case. Smaller fibers tend to have a smaller numerical apertures. A smaller numerical aperture retains more of the light closer to the fiber axis and would therefore cause more light to successfully cross the splice region thus counteracting the increase in loss created by a smaller core diameter. This is in fact what we see in experiment. It should be noted that smaller NA fibers will, however, suffer proportionally greater losses due to lateral misalignment.

A sensor was fabricated using 50/125 micron fiber whose numerical aperture was 0.20. Its initial gap was very nearly zero. As illustrated in Figure 5-4 the power decreased much like the preliminary experiments in section 5.1 predicted. A nearly flat region followed by quasi linear attenuation. This flat region is expected for a sensor with a nearly zero initial gap. As the results show, the effect of smaller core diameter

appears, to some extent, to be counteracted by the smaller numerical aperture.

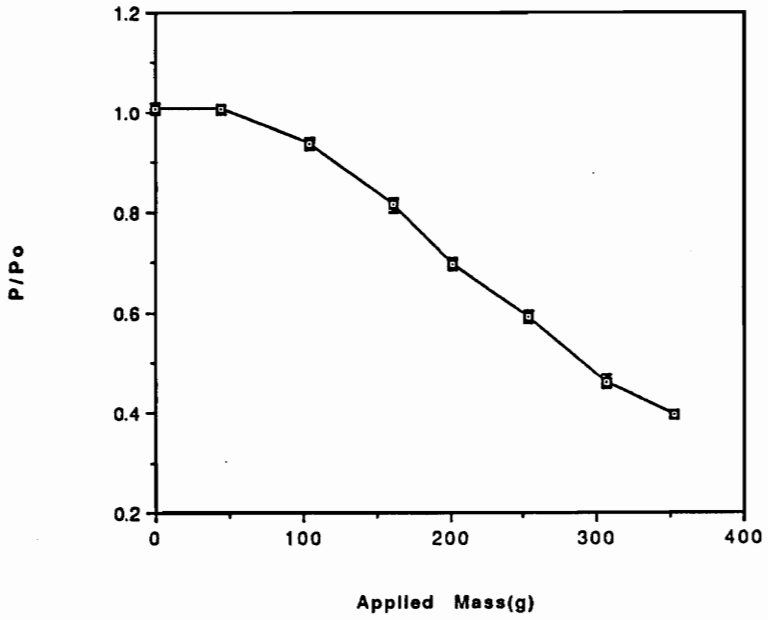

Figure 5-4. Applied mass vs. power; smaller core diameter

5.4 Effect of Gauge Length on Sensitivity.

One of the most attractive features of this sensor concept is its capacity to operate in different load ranges. That is, by varying the length of the hollow core fiber segment, the effective gauge length, the sensor can be custom tailored to the needs of a particular application. As mentioned earlier, a 10cm gauge length sensor operating over a range of 0.0 to 0.1 percent strain is expected to have the same resolution as a sensor of gauge length 1cm operating over a range of 0.0 to 1.0 percent strain. In this section experiments are performed to verify this effect.

Experiments were performed for sensors with three different gauge lengths; 10.8cm, 3.9cm and 1.0cm. These sensors were fabricated with 100/140 micron 0.28 NA fiber. In each case loads were applied to the system as seen in Figure 5-2. A zero strain value is recorded first. Subsequent power levels are then recorded as load is increased. Between each loading, a zero value is recorded to confirm the sensor's integrity and to verify that no hysterisis exists. The data is then plotted as applied mass vs. normalized power(P/P_0). These results are illustrated in Figure 5-5. As expected the slope of the curves decreases with gauge length. Therefore, for a large load range, shorter gauge length sensors may need to be used.

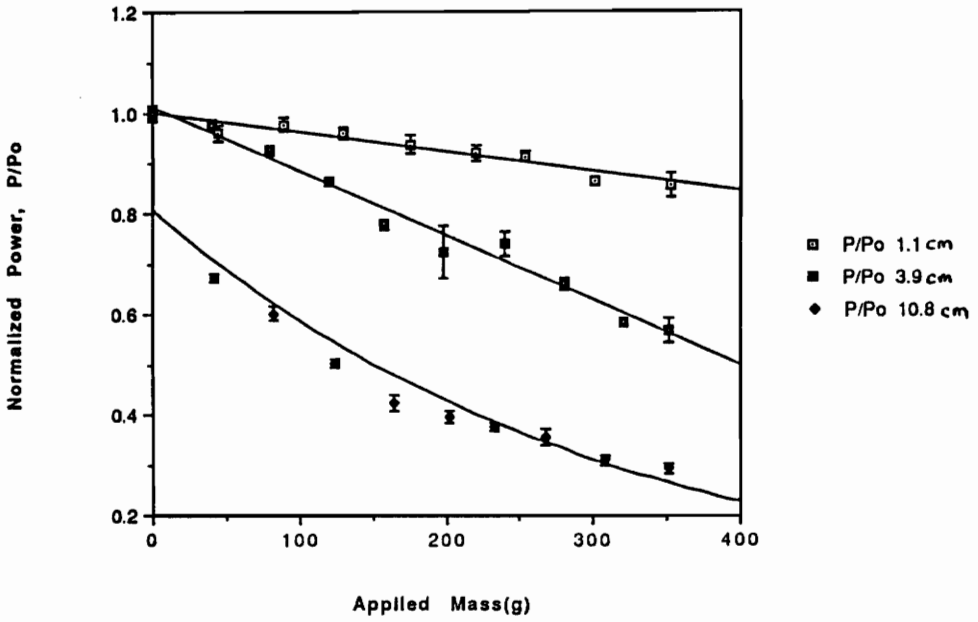

Figure 5-5. Gauge length effect on sensitivity

5.5 Launch Condition Effects on Sensitivity.

As mentioned earlier all of the leaky modes are stripped by the lossy fiber jacket For this reason these modes will not affect the sensitivity of the sensor. The modal distribution in the core, however, needs to be investigated for its potential effect on sensitivity.

Simply because we are using multimode fiber in no way insures that all modes are excited. Depending on the launch conditions, different modes will be excited and to different degrees. While the lower order modes are more tightly bound to the fiber axis the higher order modes are more easily lost. For this reason it is anticipated that a sensor with a launch condition that excites more higher order modes will be more sensitive than a sensor whose launch excites only lower order modes. The reason being that the principle of operation of the sensor dictates that light which is located on the edges of the numerical aperture as the light exits the fiber is the first to be lost in the event of longitudinal fiber misalignment. It is not known, however, to what degree this phenomenon will affect sensor performance. That is, the magnitude of perturbations to the fiber will affect the distance that it takes for the fiber to reach modal equilibrium therefore the shorter this distance the less affect launch conditions will have on sensitivity.

Data taken to document this effect is depicted in Figure 5-6. A sensor fabricated with 100/140 micron fiber with a gauge length of 1.0cm is loaded under three different launch conditions. The Photon Kinetics

FOA-1000 OTDR system offers the ability to vary the launch numerical aperture into the fiber. Experiments were performed for launch NA = 0.3, 0.2, 0.1.

It is apparent that the effect of launch conditions on sensitivity is minimal. This was a somewhat predictable result because the perturbations to the fiber and the principle of operation of the sensor both bolster modal equilibrium. Macrobending occurs throughout the optical path distance which is approximately 4 meters when operating in the reflective mode. Microbending occurs at the points where the fiber is attached to the loading apparatus as well as in the pulley region where the applied mass is attached. The most significant vehicle towards achieving modal equilibrium, however, is the splice region itself. When the light leaves the lead-in fiber it spreads out as per its numerical aperture. Therefore upon re-entering the fiber, higher order modes are excited. This process is repeated when the light is reflected back through the splice region after the far end Fresnel reflection. With all of the above factors contributing it is not difficult to understand why the distance required to achieve modal equilibrium is short. For an application where a different loading sheme is used it may be necessary to induce modal equilibrium by wrapping the lead-in fiber around a mandrel. This would insure that modal distribution did not affect sensor performance. For a sensor to be practical it must be predictable. The reduction of launch condition effects on sensor performance is a major step in this direction. The launch is simply one less variable that need be perfectly reproduced in order for the sensor to yield the predicted performance.

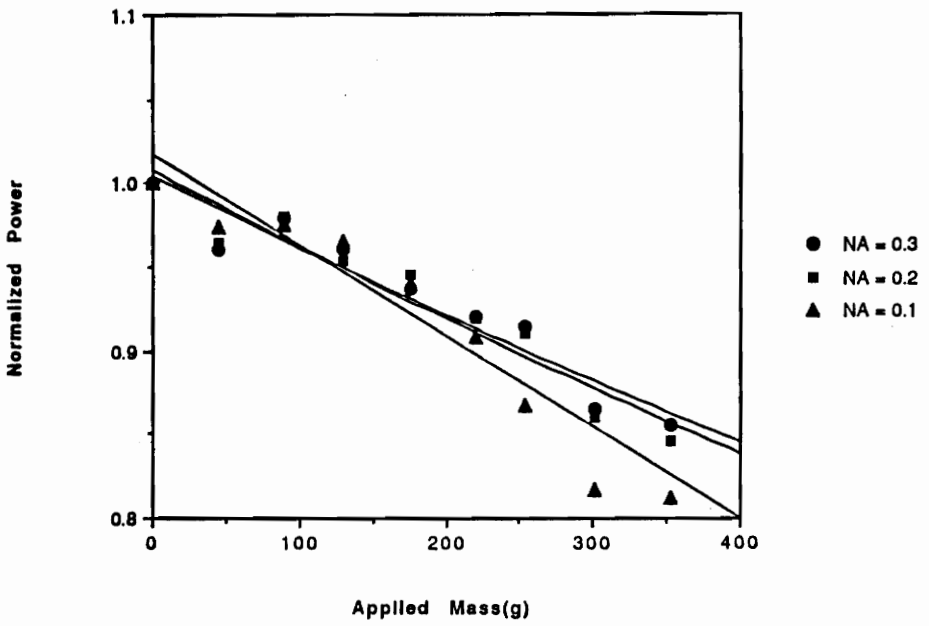

Figure 5-6. Launch condition effect on sensitivity

5.6 Lateral Misalignment.

Experiments were performed to measure the losses due to misalignment of fibers transverse to the direction of propagation. The lateral misalignment experiments were carried out in much the same fashion as the longitudinal experiments. The fibers were again aligned with a three dimensional positioner to maximize the transmitted power. The outgoing fiber was then moved in the transverse, x, direction in increments and the power levels recorded. This was done at three values of *longitudinal* separation; 0, 100, and 400 microns. This was done to see what kind of effect lateral misalignment will have in the *longitudinal* operating region of the sensor. Figure 5-7 illustrates the results of these experiments.

Because lateral misalignment is kept to within a very few microns by the hollow core fiber, this loss mechanism was not anticipated to effect the sensor performance appreciably. Further, it is found that during tensile loading, lateral misalignment is not only small but stays relatively constant further reducing any distortion of results from this effect.

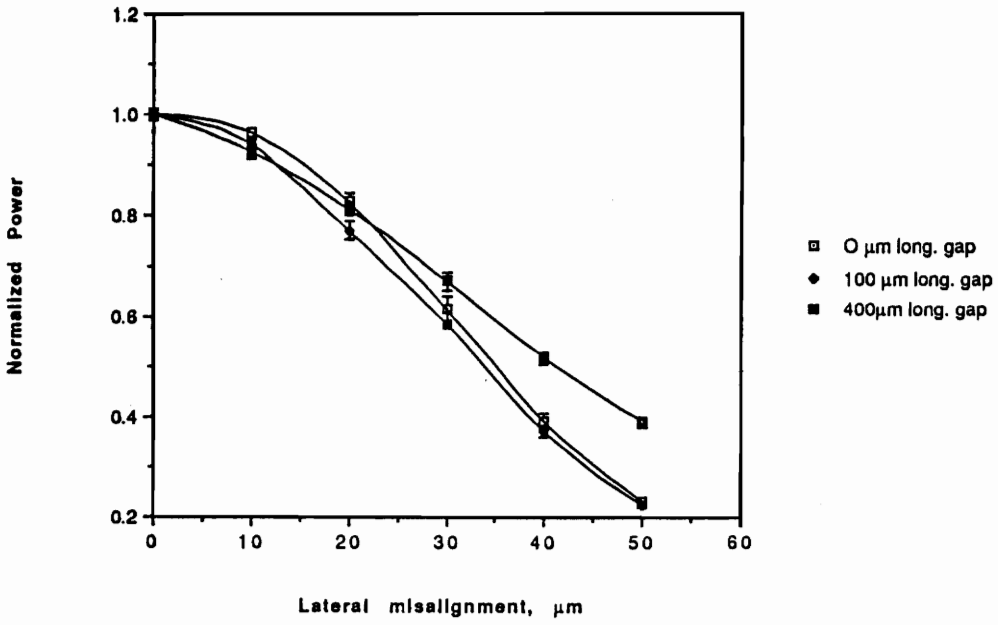

Figure 5-7. Lateral misalignment loss

6.0 RECOMMENDATIONS FOR FUTURE WORK.

As a result of the work presented in this thesis, certain supplemental experiments are recommended. It is proposed that the sensor be embedded for graphite composite strain testing. The sensor has already proven to be sensitive to strains typical of those experienced by composite structures. It is anticipated that a gauge length of 1 to 2 centimeters will provide the best sensitivity over these load ranges.

In the interest of trying to increase sensitivity it is proposed that experiments be conducted with fibers of different core diameters, i.e. two identical fibers but of core diameters different from those investigated in this work. These experiments should include fibers with different core diameters as well as with different index profiles. To be able to perform many of these experiments, new sizes of hollow core fiber may need to be drawn. The use of mismatched fibers to create the sensor should also be investigated.

7.0 CONCLUSION.

In this thesis an effective, practical strain sensor has been presented. It has been demonstrated that the longitudinal misalignment of fibers within a hollow core fiber is, in fact, a viable approach to sensing. Further, it has been shown that a practical sensor can be fabricated using this concept. Other loss mechanisms that exist in fiber interconnections have been investigated as to their potential effect on sensitivity and these effects have proven to be tolerable.

As was illustrated in Chapter 5, theory to a large extent does not agree with what was observed in the laboratory. As was mentioned earlier, it is the opinion of several authors that this discrepancy is due largely to assumptions made in simplifying the theoretical calculations. A somewhat imprecise comparison can be made, however, between the experiments for longitudinal loss and the actual strain measurements. The applied mass vs. induced strain equation is:

$$dL/Lo = mg/AE \qquad (7.1)$$

where mg is the gravitational force from the applied mass, A the area of the hollow core fiber and E Young's modulus of the hollow core fiber. This equation is used to calculate the induced fiber separation from a given applied mass. This value is then added to the initial fiber end separation to arrive at the actual fiber separation. This is a somewhat crude comparison because both the initial fiber separation and the *inner* diameter of the hollow core fiber cannot be measured with a high degree of accuracy. This comparison is depicted in Figure 7-1. A reasonably good correlation exists between the curves. For actual sensor operation one would need only the slope and initial, zero strain value, of P/Po.

This sensor has satisfied the design considerations set forth at the inception of the research; these being reasonable cost, adequate sensitivity, mass producibility and repeatability. Further, this sensor is versatile in that its sensitivity can be tailored to meet the needs of a specific application. The design of the sensor also lends itself well to embedded applications.

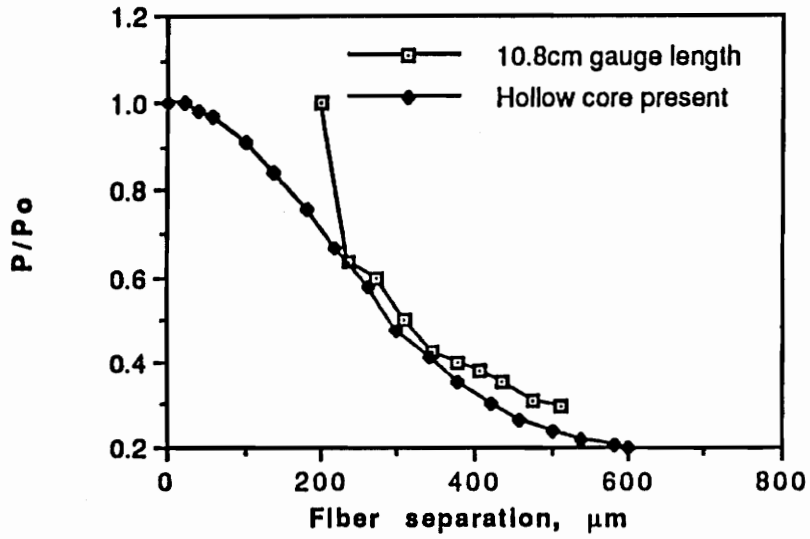

Figure 7-1. Comparison of calculated gap with known gap

REFERENCES

[1] *Bernd D. Zimmermann, "High Resolution Optical Time Domain Reflectometry and its Applications", Master's Thesis, Virginia Polytechnic Institute and State University, February, 1988.*

[2] *J.D. Weiss, "Fiber-Optic Strain Gauge," Journal of Lightwave Technology, Vol. 7, No. 9, pp. 1308-1317, Sept. 1989.*

[3] *W.B. Spillman, Jr., R.L. Gravel, "Moving fiber-optic hydrophone," Optics Letters, Vol. 5, No. 1, pp. 30-31, Jan. 1980.*

[4] *Omega Engineering, Inc. specifications sheet. Sensor type 6/120LY41.*

[5] *F.L. Thiel, R.M. Hawk, "Optical Waveguide cable connection," Applied Optics, Vol. 15, No. 11, pp. 2785-2791, 1976.*

[6] *Spectran Corporation data sheet. Fiber ID D4320010310464*

[7] *P.DiVita, U.Rossi, "Theory of coupling between multimode optical fibres," Optical and Quantum Electronics, Vol. 10, pp. 107-117, 1878.*

[8] *Op.Cit. P. DiVita, U. Rossi*

[9] *C.M. Miller, S.C. Mettler, "A loss model for parabolic-profile fiber splices," Bell System Technical Journal, Vol. 57, No. 9, November, 1978.*

[10] *Op.Cit. P. DiVita, U. Rossi*

[11] Designer's Guide to Fiber Optics, *AMP Incorporated, Harrisburg, PA, pp. 53-59, 1982.*

[12] *Op.Cit. P. DiVita, U. Rossi*

[13] *Op.Cit. P. DiVita, U. Rossi*

[14] *Op.Cit. P. DiVita, U. Rossi*

[15] *Op.Cit. F.L. Thiel, R.M. Hawk*

[16] *Op.Cit. P. DiVita, U. Rossi*

[17] *Op.Cit. Chu, McCormick*

[18] *Op.Cit. F.L. Thiel, R.M Hawk*

[19] *D. Marcuse,* Theory of Dielectric Optical Waveguides, *Academic Press, New York, p.75, 1974.*

[20] *Op.Cit. D. Marcuse*

[21] *D. Gloge, "Weakly guiding fibers," Applied Optics, Vol. 10, pp. 2252-2258, 1971*

[22] *Op.Cit. P. DiVita, U. Rossi*

[23] *D. Gloge, "Offset and Tilt Loss in Optical Fiber Splices", Bell System Technical Journal, Vol. 55, No. 7, pp. 2231-2243, September 1976.*

VITA

Jeffrey Pratt Andrews was born on May 30, 1966 in Rio de Janiero, Brazil. He is the last of four sons born to this State Department family. After two years in Brazil his family returned to the United States to his hometown Bethesda, Maryland. He lived there for the next three years and then moved to Buenos Aires, Argentina for a two year stay. In 1972 his family returned to Bethesda for good. Jeff graduated from Walt Whitman High School in 1984. Jeff spent the following four years at the State University of New York at Binghamton where he earned a Bachelors of Science degree in Physics. In the fall of that year, 1988, Jeff enrolled at Virginia Tech where he would receive a Masters of Science degree in Electrical Engineering 16 months later.